Theoretical and Experimental Studies on Vortex Chamber Flows

G. H. Vatistas,* S. Lin,† and C. K. Kwok‡
Concordia University, Montreal, Canada

Analytical and experimental studies to investigate selected fluid parameters in vortex chambers are presented. From the analytical model, the dimensionless quantities of the core size, static pressure drop across the chamber, and radial static pressure distribution are shown to be functions of the chamber geometry only. Experimental results confirm all of the findings.

Nomenclature

A_0 = cross-sectional area of the chamber
e_r, e_θ, e_z = unit vectors in r, θ, and z directions
P = static pressure
P_a = ambient pressure
Q = volumetric flow rate
q = total velocity vector $(e_r V_r + e_\theta V_\theta + e_z V_z)$
R_C = core radius
R_E = radius of the throat
R_0 = radius of the chamber
r, θ, z = independent variables, see Fig. 4b
V_r, V_θ, V_z = fluid velocity in radial, circumferential, and axial directions, respectively
$\bar{z}$ = distance from the bottom plate/height of the chamber
Γ = strength of the vortex
η, ζ, ξ = vorticities in r, θ, and z directions
θ' = pitch angle
ρ = fluid density
ψ' = yaw angle

Subscripts

D,E,F,in = properties evaluated on D, E, F, and in planes, respectively, see Fig. 4.

Introduction

THE importance of vortex flows in fluid dynamics, as well as in related fields, has preoccupied research efforts for a long period. The continuous interest on confined swirling flows, in particular, has been stimulated by the large number of engineering applications utilizing these phenomena. They range from a simple swirl atomizer[1] to a gas core nuclear rocket[2] for advanced space propulsion. Swirling motion has also been extensively used in gas turbine engines as a mean to anchor the flame in the primary zone.[3,4] Lately, the successful attempt to burn low calorific value fuels in cyclone chambers[5-7] has raised the interest to further explore confined vortex flows.

The advantages of cyclone combustors, in comparison with the conventional systems, lie mainly on the strong centrifugal force field that greatly alters the fluid motion and aids the combustion processes in two ways: 1) it enhances the residence time of the solid fuel and allows it to burn before it exits the chamber; and 2) the generated secondary flows create favorable conditions for the combustion of a waste gas. Both are achieved at the expense of pressure loss.

An extensive review by Lewellen[8] has cited a number of papers dealing with confined vortex flow phenomena. The nonlinear character of the governing equations, coupled with the complex boundary conditions, make the mathematical solution of these flows a formidable task. Consequently, only a few simple cases have been analyzed to date.

It is well known that the circumferential velocity of the confined fluid changes from a free to a forced vortex as the flow approaches the axis of rotation. Lewellen[8] determines the point of maximum tangential velocity for a liquid filled cylindrical chamber utilizing the method of Binnie and Hookings.[9] A gaseous core with a constant static pressure equal to the ambient is assumed in his analysis. Recently, Shakespear and Levy[10] reported new analytical and experimental findings for the static pressure drop across a vortex chamber. Their theoretical study showed a fair agreement of the pressure with the experiment and an overestimated radius of maximum tangential velocity.

Experimental and analytical investigations are presented in this paper. Based on the equations of motion and energy, with neglected viscous effects, the point of maximum tangential velocity is obtained. Then the pressure drop across the chamber is determined. The study shows that the dimensionless core size, pressure drop, and radial pressure distribution depend solely on the geometrical parameters of the chamber. All of the analytical findings compared favorably with the present experimental results as well as with the results of Shakespear and Levy.[10]

A General Description of the Problem

In general, vortex chambers have a cylindrical configuration with a central axis outlet and circumferential inlets. As the fluid enters through the tangential inlet port, it creates a centrifugal field and produces a flow pattern similar to the one shown in Fig. 1. Upon entering the chamber, the fluid is immediately confronted by a strong centrifugal force. In the attempt to find paths leading to the outlet with the least resistance, it is divided into two streams. The first propagates along the circumferential wall and is then directed to the outlet at a point near the bottom plate. The familiar eddy motion in the lower corner is noticeably present. The second stream flows toward the central axis through an area close to the top plate. On both paths chosen by the fluid, the tangential velocity is reduced through a boundary layer, thus diminishing the centrifugal force acting in these regions. One expects the second stream to exit the chamber through an area close to the central axis, where the centrifugal acceleration is minimum. But the static pressure has dropped well below the ambient and the induced reverse flow forces the

Presented as Paper 84-1548 at the AIAA 17th Fluid Dynamics, Plasma Dynamics and Lasers Conference, Snowmass, CO, June 25-27, 1984; received Dec. 26, 1984; revision received July 14, 1985.

*Assistant Professor, Mechanical Engineering, Department of Mechanical Engineering. Member AIAA.
†Professor of Engineering, Department of Mechanical Engineering.

stream to reach the outlet at a larger radius. Between the two streams, a toroidal recirculating flow area exists, which is similar to the secondary flow through bends.

Experimental Apparatus and Procedure

The present experiments have been conducted in Concordia's isothermal cyclone chamber. The chamber has a cylindrical shape with constant cross-sectional area with a radius R_0 of 15.24 cm and a height H of 45.72 cm. Swirl is imparted to the fluid by four identical inlet ports, 90 deg apart, located around the lower periphery of the chamber, with a total inlet area A_{in} of 68.75 cm^2. Along the circumferential wall, six openings were drilled into which the probe is easily inserted. A pressure seal into each opening is fitted to avoid air leakage. The modular construction of the top plate incorporates several concentric rings to allow the variation of the exit port.

The instrumentation system used for the present experiments is schematically illustrated in Fig. 2. As it can be seen, air from the supply line passes through two variable-area rotameters (A and B) connected in parallel. Before the air is expanded to the main chamber the static pressure difference $\Delta P(P_{in} - P_a)$ is recorded with the aid of the inclined manometer C. The three-dimensional character of the flow inside the chamber, realized in preliminary experiments, requires measuring instruments that can sense the magnitude of the mean velocity as well as its direction. Among the simplest instruments that can perform the task is the five hole pitot-probe. For the present experiments, the three-dimensional United Sensor and Control Corporation probe (model DA-125) with prismatic head was selected for velocity and static pressure mapping of the flowfield. The movement of the probe is manually controlled by the traversing mechanism E, which is readable within an accuracy of ± 0.127 cm (± 0.05 in.). The yaw angle of the probe is determined via an adjustable disk dial graduated in intervals of 0.5 deg. The static pressures are recorded by the sensitive inclined manometers F and G.

For a typical experimental run several steps are followed. First, the probe is inserted in the chamber at a specific axial station where the radial traverse is needed and it is aligned carefully with the radius. The reference angle is established to be zero when pressure tap 1 (see Fig. 3) is aligned with the central axis of the chamber. The desired flow rate is selected and read from flow meters A and B. Approximately 15 min are allowed to elapse prior to any reading, in order for the flowfield to achieve steady-state conditions. The pitot probe is rotated about its axis until pressures 2 and 3 are balanced and the yaw angle ψ' is recorded from the circular protractor. At this stage, pressure tap 1 has been aligned with the projection of the total velocity vector q in the V_z and V_θ planes. The pressures from taps 1, 4, and 5, are recorded. The pressure coefficients are then calculated and the total pressure and pitch angle are obtained from the calibration charts. From Bernoulli's equation, the total velocity at the point is determined. The velocity components at the point are calculated using simple trigonometric relations. The probe is then moved to the next point and the process is repeated until a complete traverse at the desired axial station is made. However, when using the probe in taking the

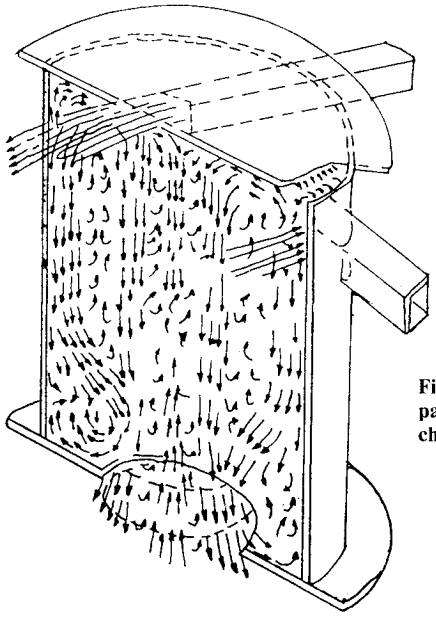

Fig. 1 Typical flow pattern in a vortex chamber (from Ref. 11).

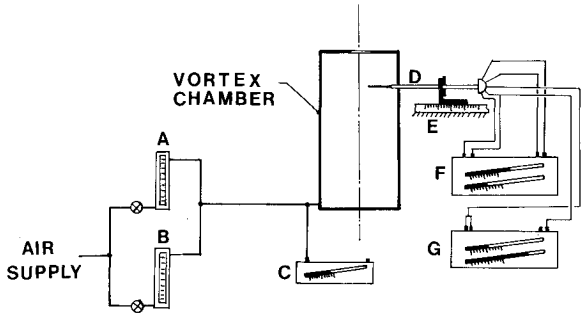

Fig. 2 Experimental apparatus.

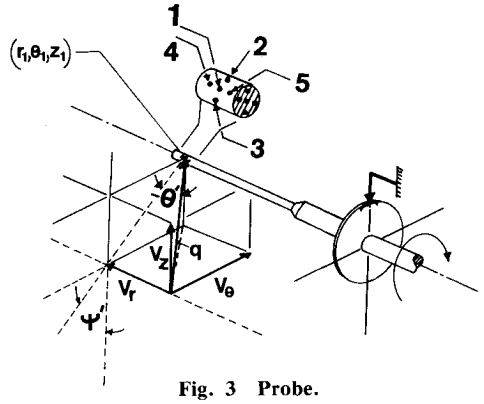

Fig. 3 Probe.

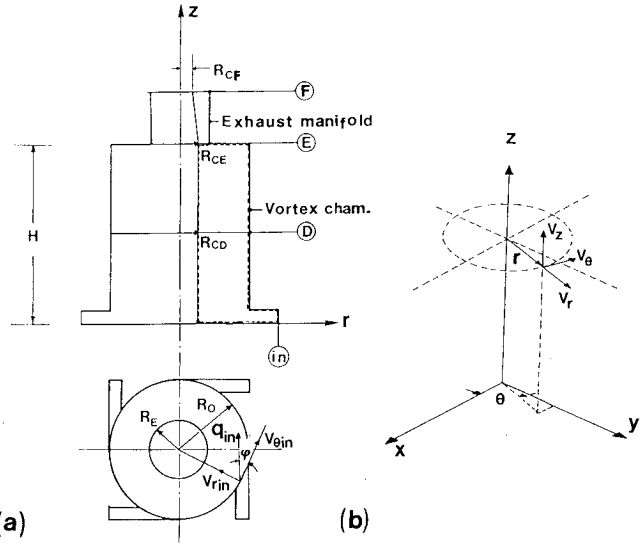

Fig. 4 a) Schematic of the physical problem. b) Coordinate system.

measurements, extreme care must be exercised to minimize the adverse effects thoroughly discussed in Refs. 4 and 8.

The data obtained are fed into a computer program and the velocities are plotted utilizing printing and cubic spline routines. The radius of maximum tangential velocity is graphically determined as the point where the radial gradient of V_θ is zero.

Governing Equations

Consider the steady flow of an incompressible and inviscid fluid inside the vortex chamber depicted in Fig. 4 with exaggerated exhaust manifold. The equations for the flow are

Momentum

$$\nabla\left(\frac{P}{\rho}+\frac{q^2}{2}\right)+q\times\text{curl}q=0 \tag{1}$$

Continuity

$$\nabla\cdot q=0 \tag{2}$$

where the vorticity is defined as

$$\text{curl}q=e_r\xi+e_\theta\eta+e_z\zeta$$

The vorticity components of the axisymetric flow in cylindrical coordinates are

$$\xi=-\frac{\partial V_\theta}{\partial z},\quad \eta=\frac{\partial V_r}{\partial z}-\frac{\partial V_z}{\partial r},\quad \zeta=\frac{\partial V_\theta}{\partial r}+\frac{V_\theta}{r} \tag{3}$$

For a potential flow, the vorticity is zero and Eq. (1) gives the Bernoulli equation.

It is interesting to note that if the continuity equation and the equation for the η vorticity component are combined into a single equation with the aid of the stream function, the resulting equation will not contain the velocity component in θ direction. This suggests that, for the potential flow, fluid motion in the r and z directions is taking place although V_θ is absent. However, it should be noted that the potential flow assumption outside the core region in the vortex chamber is only an approximation.

Core Size and Pressure Drop Across the Chamber

Experimental results shown in Fig. 5 indicate that the radius where the maximum tangential velocity occurs, does not vary significantly along the height of the chamber. This is also evident from the experimental studies of Reydon and Gauvin[12] and Ogawa.[13] In view of this experimental evidence, the core is assumed to be constant within the vortex chamber. In the present study, the core is defined as the space bounded by a cylindrical surface having the same radius with the point of maximum tangential velocity. The potential flow is assumed to take place in the region outside the core in the control volume, illustrated in Fig. 4 by dashed lines. In the flow volume inside the exhaust manifold, the potential theory cannot be applied, since the condition of a constant static pressure at the exit of the manifold cannot be met.

For the assumed potential flowfield, the energy equation is expressed by,

$$P/\rho+q^2/2=\text{const} \tag{4}$$

Equation (4) implies that every point in the field has the same total energy. Application of Eq. (4) between the inlet and at any radius on E yields,

$$\frac{P_E}{\rho}+\frac{q_E^2}{2}=\frac{P_{in}}{\rho}+\frac{q_{in}^2}{2} \tag{5}$$

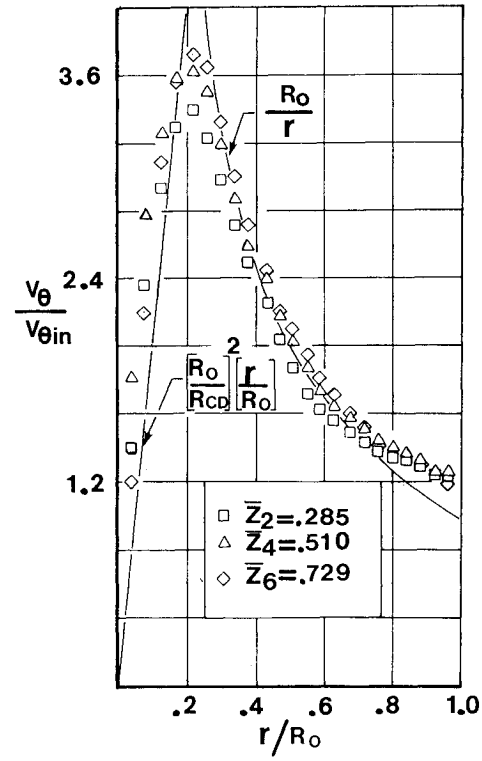

Fig. 5 Experimental tangential velocity distribution for different axial stations ($\bar{z}$ = distance from bottom plate/height of chamber).

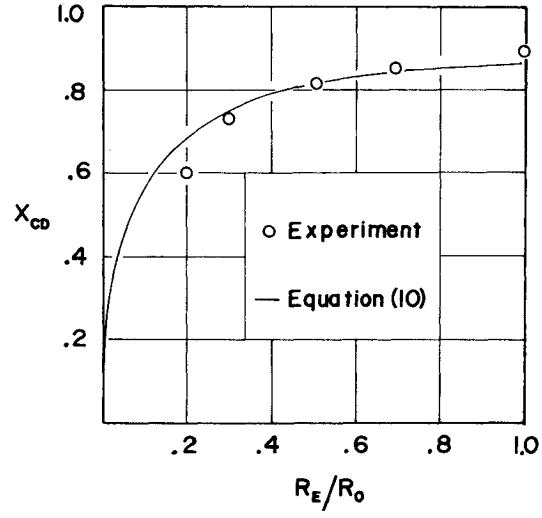

Fig. 6 Core size on D plane for different R_E/R_0 (for the axial station $\bar{z}_4$).

To simplfy the problem it is assumed that

$$V_{rE}\cong 0$$

From the η vorticity, Eq. (3) becomes

$$V_{zE}=\text{const}$$

It should be noted that P_{in} and q_{in} are uniform at the inlet, while P_E and q_E are functions of the radius. Then, Eq. (5) gives

$$\frac{2(P_{in}-P_{CE})}{\rho}=\left(\frac{\Gamma}{2\pi R_{CE}}\right)^2+V_{zE}^2-q_{in}^2 \tag{6}$$

Continuity gives

$$Q = V_{zE}\pi(R_E^2 - R_{CE}^2) = |q_{in}|A_{in} \tag{7}$$

Substitution of Eq. (7) into Eq. (6) yields

$$\frac{2\Delta P_E}{\rho} = \left(\frac{Q}{\pi R_E^2}\right)^2 \frac{1}{(1-X_{CE}^2)^2} + \left(\frac{\Gamma}{\pi R_E}\right)^2 \frac{1}{4X_{CE}^2} - \left(\frac{Q}{A_{in}}\right)^2 \tag{8}$$

where $\Delta P_E = P_{in} - P_{CE}$ and $X_{CE} = R_{CE}/R_E$.

For given values of Q, A_{in}, R_E and Γ, one obtains from Eq. (8),

$$\lim_{X_{CE}\to 0}\left(\frac{2\Delta P_E}{\rho}\right) = \infty \quad \text{and} \quad \lim_{X_{CE}\to 1}\left(\frac{2\Delta P_E}{\rho}\right) = \infty$$

From the above, it is evident that there must be an X_{CE}, in $0 < X_{CE} < 1$, such as to minimize the pressure difference or,

$$\frac{\partial}{\partial X_{CE}}\left(\frac{2\Delta P_E}{\rho}\right) = 0 \tag{9}$$

Under Eq. (9), Eq. (8) becomes

$$X_{CE}^6 + (2a-3)X_{CE}^4 + 3X_{CE}^2 - 1 = 0 \tag{10}$$

where

$$a = \left[\frac{(A_{in}/A_0)}{(R_E/R_0)\cos\varphi}\right]^2$$

and

$$A_0 = \pi R_0^2$$

In order to determine the core size at the exit of the exhaust manifold (F plane), some assumptions have to be made, as

1) The experimental results obtained by Shakespear and Levy[10] have shown that the axial velocity at the exit of their vortex chamber can be assumed constant and to extend as far as R_{CF}. For the present analysis this assumption is also adopted.

2) At the exit of the manifold, the radial velocity is relatively small in comparison with the axial and tangential components and may be neglected.

Application of the integral energy equation to the flow bound by the core, the circumferential wall, the inlet and outlet of the exhaust manifold, with neglected viscous dissipation effects, gives

$$2\pi\int_{R_{CF}}^{R_E}\left[\frac{P_a}{\rho} + \frac{1}{8}\left(\frac{\Gamma}{\pi r}\right)^2 + \frac{1}{2}V_{zF}^2\right]V_{zF}r\,dr = \left(\frac{P_E}{\rho} + \frac{1}{2}q_E^2\right)Q = \left(\frac{P_{in}}{\rho} + \frac{1}{2}q_{in}^2\right)Q \tag{11}$$

where P_E and q_E are functions of the radius.

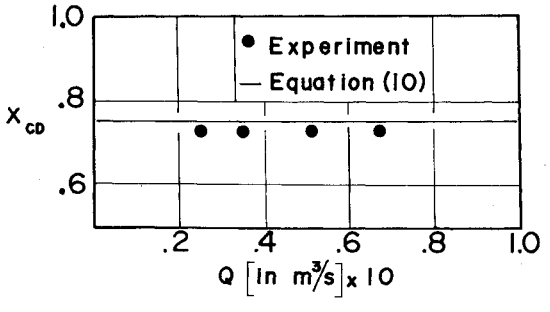

Fig. 7 Core size vs Q ($R_E/R_0 = 0.3$).

Integration of Eq. (11) yields,

$$\Delta P = \frac{\rho}{2}\left[\left(\frac{Q}{\pi R_E^2}\right)^2 \frac{1}{(1-X_{CF}^2)^2} + \frac{1}{2}\left(\frac{\Gamma}{\pi R_E}\right)^2 \frac{\ell n(1/X_{CF})}{(1-X_{CF}^2)} - \left(\frac{Q}{A_{in}}\right)^2\right] \tag{12}$$

where $\Delta P = P_{in} - P_a$ and $X_{CF} = R_{CF}/R_E$.

Minimization of Eq. (12) with respect to X_{CF} gives,

$$X_{CF}^4(2\ell n X_{CF} - 1) + 2X_{CF}^2[(a+1) - \ell n X_{CF}] - 1 = 0 \tag{13}$$

The pressure difference across the chamber ΔP can be then expressed in dimensionless form as

$$\overline{\Delta P} = \left[\left(\frac{A_{in}}{\pi R_E^2(1-X_{CF}^2)}\right)^2 - 1\right]\frac{1}{\sin^2\varphi} - \frac{2\ell n X_{CF}}{(R_E/R_0)^2\tan^2\varphi(1-X_{CF}^2)} \tag{14}$$

where $\overline{\Delta P} = 2\Delta P/\rho V_{in}^2$.

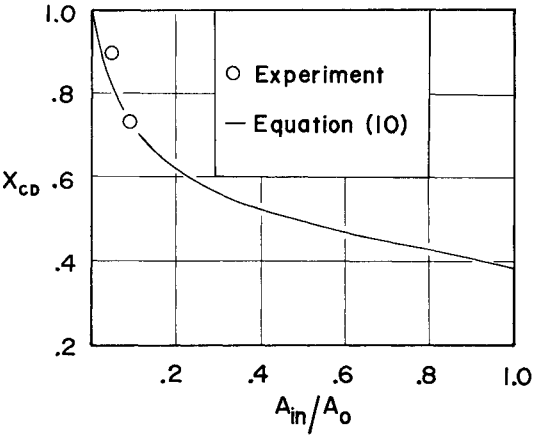

Fig. 8 Variation of X_{CD} with the total inlet area ($A_0 = \pi R_0^2$, $R_E/R_0 = 0.3$).

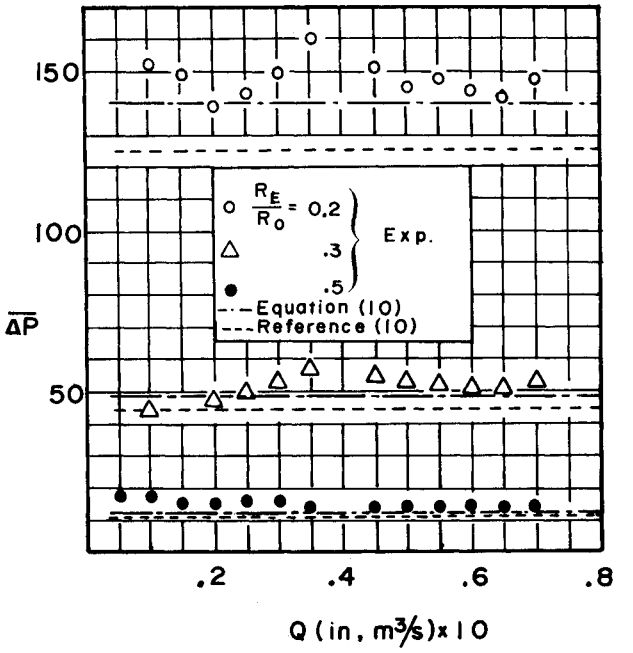

Fig. 9 Variation of the dimensionless pressure drop across the chamber with the volumetric flow rate for three contraction ratios.

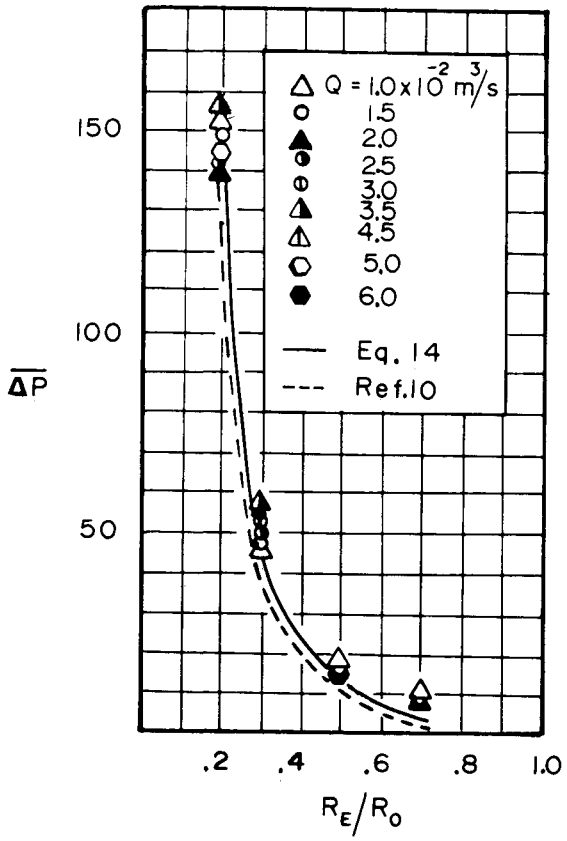

Fig. 10 Dimensionless pressure drop across the chamber vs contraction ratio.

Applying Eq. (4) between the wall ($r=R_0$) and any radius in the region $R_{CE} \le r < R_0$ and assuming $V_{zD}=\text{const}$, $V_{rD}=0$, and $R_{CD}=R_{CE}$ one gets

$$P_D(r) = P_D + \frac{\rho}{8}\left(\frac{\Gamma}{\pi R_0}\right)^2\left[1-\frac{1}{(r/R_0)^2}\right] \tag{15}$$

However,

$$P_D = P_{in} + \frac{\rho}{2}\left[q_{in}^2 - V_{zD}^2 - \left(\frac{\Gamma}{2\pi R_0}\right)^2\right] \tag{16}$$

Then, with the aid of Eqs. (14) and (16) and the continuity, after some tedious algebraic manipulations, Eq. (16) becomes,

$$\overline{\Delta P_D} = \frac{(A_{in}/A_0)^2}{(R_E/R_0)^4(1-X_{CF}^2)^2}\left\{1-\left[\frac{1-X_{CF}^2}{(R_0/R_E)^2-X_{CE}^2}\right]^2\right\}\sec^2\varphi - \left[\frac{2\ell n X_{CF}}{(R_E/R_0)^2(1-X_{CF}^2)}+\frac{1}{(r/R_0)^2}\right]\cot^2\varphi \tag{17}$$

where $\overline{\Delta P_D} = 2[P_D(r)-P_a]/\rho V_{in}^2$.

Following the same line of argument, the dimensionless radial pressure distribution on the E plane is

$$\overline{\Delta P_E} = \frac{(A_{in}/A_0)^2}{(R_E/R_0)^4(1-X_{CF}^2)^2}\left\{1-\left[\frac{1-X_{CF}^2}{1-X_{CE}^2}\right]^2\right\}\sec^2\varphi - \left[\frac{2\ell n X_{CF}}{(R_E/R_0)^2(1-X_{CF}^2)}+\frac{1}{(r/R_0)^2}\right]\cot^2\varphi \tag{18}$$

where $\overline{\Delta P_E} = 2[P_E(r)-P_a]/\rho V_{in}^2$.

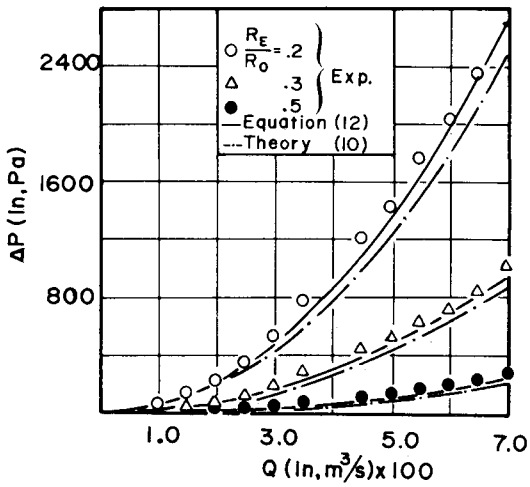

Fig. 11 ΔP vs Q for three different contraction ratios.

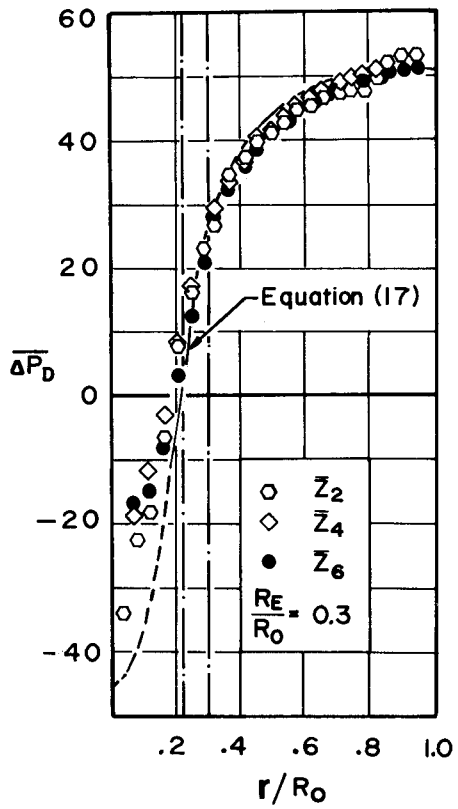

Fig. 12 Static pressure distribution inside the chamber ($Q=0.035$ m^3/s).

The following facts should be noted:

1) The dimensionless core size on the throat and the exit planes [Eqs. (10) and (13)] depend solely on the geometrical parameter a.

2) Both equations satisfy the limiting cases,

$$X_{CE}, X_{CF} \to 0 \text{ when } \Gamma \to 0$$

$$X_{CE}, X_{CF} \to 1 \text{ when } \Gamma \to \infty$$

3) The dimensionless pressure drop across the chamber [Eq. (14)] and pressure radial distribution on the D and E planes [Eqs. (17) and (18), respectively] are functions of only the geometric parameters of the chamber.

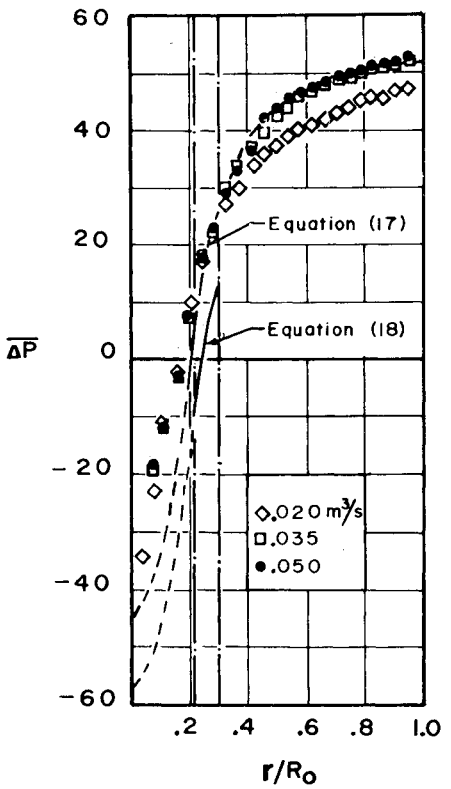

Fig. 13 Static pressure distribution for different planes ($R_E/R_0 = 0.3$).

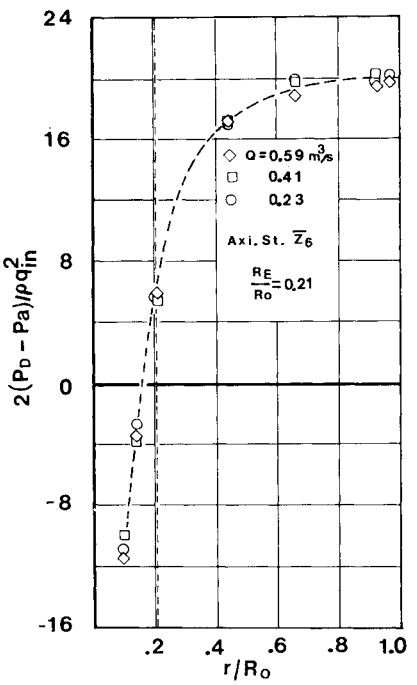

Fig. 14 Experimental static pressure distribution inside the vortex chamber from Ref. 12 ($\bar{z}_6 = 0.56$).

Results and Discussions

Results of the analysis presented in the previous section are now compared with the experimental data.

Analytical and experimental results of the core size as a function of the contraction ratio (R_E/R_0) are presented in Fig. 6. The core size is seen to be strongly dependent on the ratio R_E/R_0, especially for smaller values of the latter. The smaller the contraction ratio, the lesser the dimensionless

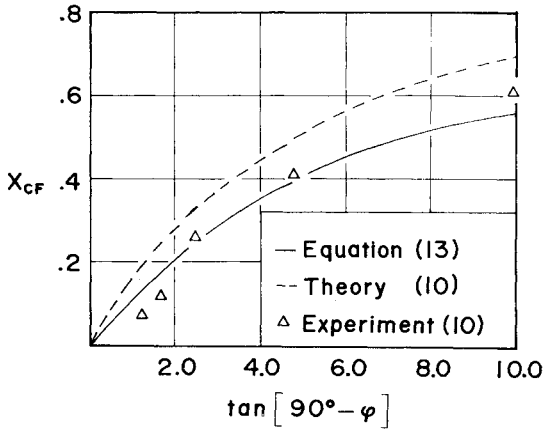

Fig. 15 Core size on exit plane vs inlet swirl ($R_E/R_0 = 0.333$).

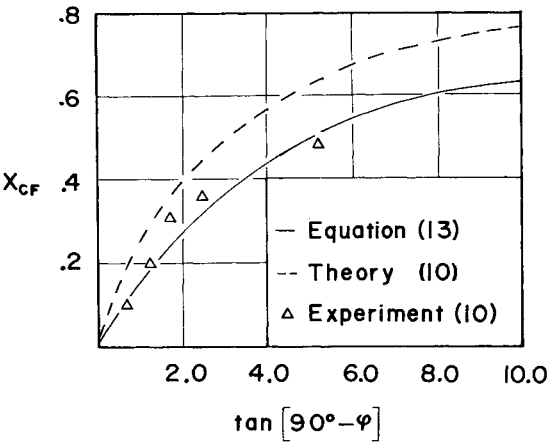

Fig. 16 Core size on the exit vs inlet swirl ($R_E/R_0 = 0.5$).

core size inside the chamber. In effect, this implies a larger potential flow area, which results into a larger pressure drop from the wall to the core (as shown below in Figs. 12 and 13). A further decrement of the static pressure inside the core, due to solid-body rotation (shown in Figs. 12 and 13 by dashed lines) will result into a reverse flow near the axis of rotation. The independence of X_{CD} with the volumetric flow rate, as indicated by Eq. (10), is confirmed by experimental data as depicted in Fig. 7. This is also evident from the experimental results reported in Ref. 12. Unfortunately, no detailed information concerning the inlet boundary conditions is given, thereby no quantitative comparison of the present theory with the experiment of Ref. 12 is possible. Nevertheless, the analytical finding is qualitatively in agreement with the latter experiment.

The influence that the ratio of the inlet area to the cross-sectional area of the chamber has on the core size is shown in Fig. 8. The two experimental points given in the graph correspond to areas A_{in} of 68.70 and 34.37 cm^2. Because of fixed inlet area ports, it was possible to obtain only two experimental points with the aid of restrictions inserted at the inlets. The influence of small values of A_{in}/A_0 on X_{CD} is of a more moderate nature than the effect of the corresponding values of contraction ratio. Equation (14) indicates that the dimensionless pressure difference across the chamber is not a function of the volumetric flowrate. However, experimental data presented in Fig. 9 shows a small fluctuation of the dimensionless pressure about a mean value. Nevertheless, the agreement between theory and experiment is reasonably

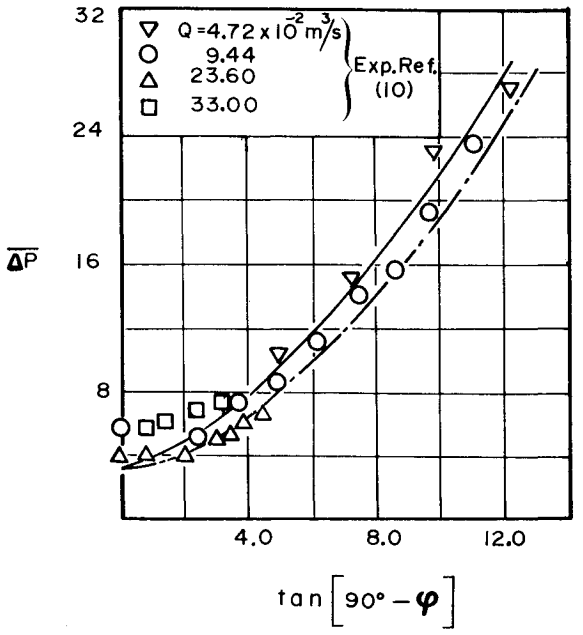

Fig. 17 Dimensionless pressure drop across the chamber vs inlet swirl ($R_E/R_0 = 0.333$, —— present theory, —·— theory from Ref. 10).

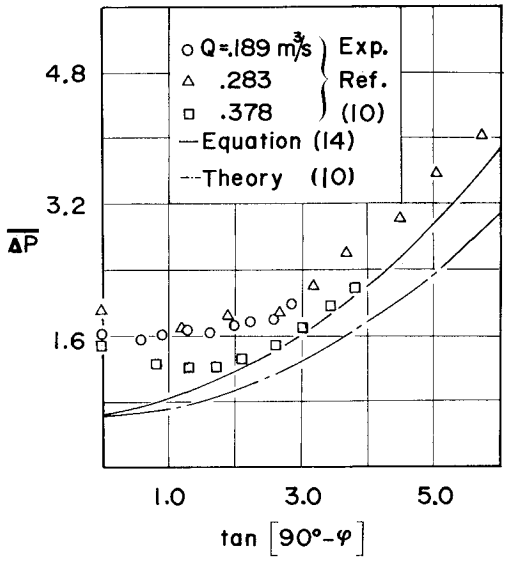

Fig. 18 Dimensionless pressure drop across the chamber vs inlet swirl ($R_E/R_0 = 0.5$).

good. Figure 10 shows a hyperbolic relation between ΔP ($\Delta P = 2\Delta P/\rho V_{in}^2$) vs the contraction ratio. When R_E/R_0 decreases, there is a drastic pressure drop increase across the chamber. The smaller the effective exit area, the higher the pressure drop ΔP. The parabolic behavior of pressure drop ΔP vs volumetric flow rate Q, depicted in Fig. 11, is similar to that of the orifice equation. The closeness of the theoretical results with the experiment justifies the assumption of negligible viscous effects. This is mainly due to the dominating effect of the centrifugal force. Styles et al.[5] have also experimentally obtained the variation of the pressure drop across the chamber vs the Reynolds number, which is based on the exit diameter, for three different inlet areas. The experimental ΔP vs Q curves presented in Ref. 5 are similar to those of Fig. 11. In addition, they show a decrease in pressure drop ΔP for larger inlet areas. The latter experimental evidence of Ref. 5 can be explained based on Eqs. (13) and (14). As the inlet area increases, the values of X_{CF} decreases. The effective outlet area becomes larger, thereby causing a small ΔP across the chamber.

The experimental dimensionless radial pressure distribution for the axial stations $\bar{z}_2$, $\bar{z}_4$, and $\bar{z}_6$ with that calculated by Eq. (17) are shown in Fig. 12. The three experimental points in every radii are seen to coincide in the interval $R_{CE} \leq r \leq R_0$. The agreement of theory with experiment is excellent, which is a further indication of the dominating behavior of the tangential velocity component. Equation (17) also suggests that the radial pressure distribution is not a function of the volumetric flow rate. This is shown in Fig. 13. With the exception of $Q = 0.02$ m^3/s, where an 11% maximum difference is shown, the rest confirms the theoretical finding. This is also evident in the experimental results of Reydon and Gauvin[12] presented in Fig. 14. If their radial pressure distributions are dimensionalized with the volumetric flow rate, all of the curves collapse into one. The pressure, from Figs. 12-14, are seen to have a maximum value on the wall decreasing toward the core radius. A further decrement of the pressure inside the core to subambient values, due to solid-body rotation given by the dashed lines, will induce the well-known suction near the axis of rotation. At the throat the non-negligible axial velocity results into a smaller value of the pressure. However, the trend on both the D and E planes is the same, since Eqs. (17) and (18) differ by a constant. Solution to Eqs. (10) and (13) gives $X_{CE} > X_{CF}$; the flow area of the exit is larger than that of the throat. Therefore, due to the area expansion, the static pressure of the fluid will recover at the exit plane at the expense of its kinetic energy.

To study the effects of swirl number ($V_{\theta in}/V_{rin}$ or tan (90 deg-φ)) on the core size and pressure drop across the chamber, the experimental results of Ref. 10 were used. The effects are depicted in Figs. 15-18. It is seen that the variation of swirl number on X_{CF} (Figs. 15 and 16) is similar to the variation of the contraction ratio. An increase of the swirl at the inlet results into an increase of the core. Higher swirl also implies reduction of the exit area, which gives a higher pressure drop (Figs. 17 and 18).

Conclusion

A theoretical analysis and experimental results concerning the core size of the confined vortex flow, pressure drop across a vortex chamber, and the pressure distribution inside the chamber are presented. The dimensionless core size, pressure drop, and radial pressure distribution are functions only of the geometric parameters of the chamber. The analysis in which the viscous effects were neglected was found to agree reasonably well with the experiment. This showed that, for a gas with sufficient swirl, the pressure drop across the chamber is mainly controlled by the centrifugal field.

Acknowledgments

This work was partially supported by the Natural Sciences and Engineering Research Council of Canada under Grant A7435. G. H. Vatistas is also grateful to the Council for the graduate scholarship awarded him during the course of this investigation. The authors are indebted to Mr. A. I. Georgantas who carried out some of the experiments.

References

[1]Beer, J. M. and Chigier, N. A., *Combustion Aerodynamics*, Applied Science, London, 1972.

[2]Love, W. L. and Park, C., "An Experiment on the MHD-Driven Rotating Flow for a Gas Core Nuclear Rocket," *AIAA Journal*, Vol. 8, Aug. 1970, pp. 1377-1385.

[3]Lilley, D., "Fluid Dynamic Combustor Research Problems," Paper presented at DOD Colloquium on Gas Turbine Combustor Modeling, Purdue University, West Lafayette, IN, Sept. 1979.

[4]Rode, D. L. and Lilley, D. G., "Mean Flowfields in Axisymmetric Combustor Geometries with Swirl," AIAA Paper 82-017, Jan. 1982.
[5]Styles, A. C., Syred, N., and Najim, S., "A Study of a Modulable Cyclone Combustor Using Gaseous Fuel," Paper presented at Spring Meeting of Central Section, The Combustion Institute, NASA Lewis Research Center, OH, March 1977.
[6]Najim, S. E., Styles, A. C., and Syred, N., "Stabilization of Low Calorific Value Gases in Cyclone Combustor," *Journal of Energy*, Vol. 5, Jan.-Feb. 1981, pp. 43-50.
[7]Krepec, T. and Kwok, C. K., "Preliminary Investigation of a Double Vortex Combustion Chamber," Paper presented at Fall Meeting of Eastern Section, The Combustion Institute, Pittsburgh, Oct. 1981.
[8]Lewellen, W. S., "A Review of Confined Vortex Flows," NASA CR-1772, July 1971.
[9]Binnie, A. M. and Hookings, G. A., "Laboratory Experiments on Whirlpools," *Proceeding of the Royal Society of London*, Ser. A, Vol. 205, 1951, p. 530.
[10]Shakespear, W. J. and Levy, E. K., "Pressure Drop in a Confined Vortex with High Flow Rate," *Conference Proceedings of the Winter Annual Meeting of ASME,* Chicago, IL, Nov. 1980.
[11]Baluev, E. D. and Troyankin, Y. V., "Study of the Aerodynamic Structure of Gas Flow in Cyclone Chambers," *Thermal Engineering*, Vol. 14, 1967, p. 99.
[12]Ryedon, R. F. and Gauvin, W. H., "Theoretical and Experimental Studies of Confined Vortex Flows," *The Canadian Journal of Chemical Engineering*, Vol. 59, Feb. 1981, pp. 14-23.
[13]Ogawa, A., "Estimation of the Collection Efficiencies of the Three Types of the Cyclone Dust Collectors from the Standpoint of the Flow Pattern in the Cylindrical Cyclone Dust Collectors," *Bulletin of Japanese Society of Mechanical Engineers*, Vol. 27, No. 223, Jan. 1984, pp. 64-69.